Physically meaningful Monte-Carlo approach to the four-flux solution of a dense multilayered system

E. DE LA HOZ[1], R. ALCARAZ DE LA OSA[1], D. ORTIZ[1], J. M. SAIZ[1], F. MORENO[1], AND F. GONZÁLEZ[1,*]

[1] *Group of Optics, Department of Applied Physics, University of Cantabria, Santander, Spain*
[*] *Corresponding author: gonzaleff@unican.es*

Compiled November 21, 2018

Due to the complexity of the radiative transfer equation, light transport problems are commonly solved using either models under restrictive assumptions, e.g., N-flux models where infinite lateral extension is assumed, or numerical methods. While the latter can be applied to more general cases, it is difficult to relate their parameters to the physical properties of the systems under study. Hence in this contribution we present, firstly, a review of a four-flux formalism to study the light transport problem in a plane-parallel system together with a derivation of equations to evaluate the different contributions to the total absorptance and, secondly, as a complementary tool, a Monte Carlo algorithm with a direct correspondence between its inputs and the properties of the system. The combination of the four-flux model and the Monte Carlo approach provides: i) all convergence warranties since the formalism has been established as a limit and ii) new added capabilities, i.e., both temporal (transient states) and spatial (arbitrarily inhomogeneous media) resolution. The support between the theoretical model and the numerical tool is reciprocal since the model is utilized to set a Monte Carlo discretization criterion, while the Monte Carlo approach is used to validate the aforementioned model. This reinforces the parallel approach used in this work. Furthermore, we provide some examples to show its capabilities and potential, e.g., the study of the temporal distribution of a delta-like pulse of light.

OCIS codes: (330.1690) Vision, color and visual optics, color; (300.1030) Spectroscopy, absorption; (290.7050) Scattering, turbid media; (260.2710) Physical optics, inhomogeneous optical media; (240.6700) Optics at surfaces, surfaces.

http://dx.doi.org/10.1364/ao.XX.XXXXXX

1. INTRODUCTION

The study of light propagation in media that scatter and absorb light has developed an interest in many different disciplines such as astronomy [1, 2], atmospheric physics [3–5] and remote sensing [6, 7] among others. These studies usually imply solving the radiative transfer equation (RTE) [8]. However, due to its complexity, many resolution techniques and approximations have been suggested. The four-flux model employed in this paper is a particular case of the N-flux model approximation to solve the RTE in systems with a plane-parallel geometry. N-flux models, firstly described by Mudgett and Richards [9], separate light into N contributions each one associated to an annular solid angle depending on its angular distribution. N can indeed be very large but models with low N present the advantage of providing simple formulae easily utilizable for macroscopic magnitudes, such as spectral reflectance or transmittance. Probably the most widely used N-model is the Kubelka-Munk (KM) model [10]. The KM model was developed to study light propagation, by splitting light into two isotropic diffuse fluxes propagating in the forward and backward direction, in painted layers. Extensions of this model include the application to fluorescing media [11], perpendicular collimated illumination under certain conditions [12], to high-absorptive media [13] or, among the most recent extensions, the applicability to media over an arbitrary substrate [14]. Due to its simplicity, it has been widely spread in many technological and industrial areas, such as the paper industry [15], the paint industry [10] or printing applications [16]. Despite its numerous applications, this model has built-in limitations, like the assumption of diffuse illumination, that causes the model to fail in providing accurate results under collimated incident illumination.

To account for collimated contributions, four-flux models in which light is decomposed into two collimated and two diffuse components traveling in the forward and backward directions were proposed. Solutions using a four-flux model of light transfer through a slab containing absorbing and scattering particles in an absorbing medium have been presented in [17], [9], [18] and [19], although the latter has become the main reference. This approach has been improved by several authors [20–22]. There are applications of this model in diverse fields such as

pigmented paintings [23], x-ray shielding [24], thermal barrier coatings [25] and nanotechnology for energy applications [26].

An extension of the model to multilayer systems using a matrix formalism was proposed in [27]. The problem of this extension is that it is not easily applicable since the addition of a layer results in the addition of new four constants which increases rapidly the complexity with the number of layers. Along analytical solutions to four-flux models, Monte Carlo (MC) approaches have been proposed [28]. A MC approach using a multilayer four-flux model to describe the radiative transfer across multiple scattering media was presented in [29]. However, the MC inputs do not have a direct relationship with the media's properties. In this paper, we put forward a MC approach based as well in a multilayer four-flux model in which the probabilities of each layer have a direct relation with the scattering and absorbing properties.

The paper is organized as follows. In section 2 we review the four-flux model in the case of an infinite lateral slab with Mie scatterers embedded including an absorbing substrate, as a generalization of the revised version presented in [14] to any combination of collimated plus diffuse incidence. Special attention is paid to the case of absorptance, for which specific expressions are shown. In section 3 a multi-layer four-flux model based MC algorithm is presented. Comparisons with theoretical results are conducted to study the conditions under which the MC yields accurate results. In particular, a fine discretization criterion and a minimum number of samples (beams) able to guarantee convergence to the theory are provided. Section 4 contains a set of numerical and theoretical results. The results selected satisfy two criteria: first, they validate the theoretical expressions derived in section 2, and second, they show some of the capabilities of the MC from its handling of the elemental beams and the possibility of analyzing them in terms of their history beyond the cumulative character of the reflectance and transmittance factors. Finally, section 5 shows the conclusions drawn from this work.

2. FOUR-FLUX MODEL REVISITED

As previously mentioned, N-flux models allow to solve the RTE in non-emitting plane-parallel media with infinite lateral extension, i.e., lateral scattering within the media is not taken into account thus the equation depends only on one spatial direction (z). Indeed, they, and the four-flux model in particular, can be derived from the scalar RTE. Although the vector RTE, which takes into account light polarization, has long been derived [30], currently there is not a derivation of N-flux models from the vector RTE. Therefore, the largest source of error of these models arises from neglecting the fact that light can be polarized. In N-flux models light intensity is divided in N solid angles in the coordinate system. In this paper, we focus in a particular case known as the four-flux model.

The four-flux model studies a system consisting of a parallel-planar medium, which embeds discrete homogeneous spherical particles, placed in optical contact with a substrate. The scattering and absorbing properties of the medium can be derived from the Mie scattering theory, as proposed in [19]. In the small particle limit, the scattering can be assumed to be isotropic. For simplicity sake, we have assumed in the following, unless stated otherwise, that the inclusions are sufficiently small so that the the isotropic scattering assumption holds.

Light propagation within the slab is modeled using the following fluxes:

- A collimated flux traveling toward positive z direction (I_c).
- A collimated flux traveling toward negative z direction (J_c).
- A diffuse flux traveling toward positive z direction (I_d).
- A diffuse flux traveling toward negative z direction (J_d).

As light is scattered within the media the total diffuse flux ($I_d + J_d$) increases at the expense of collimated fluxes. Figure 1 shows a sketch of the system and the fluxes considered.

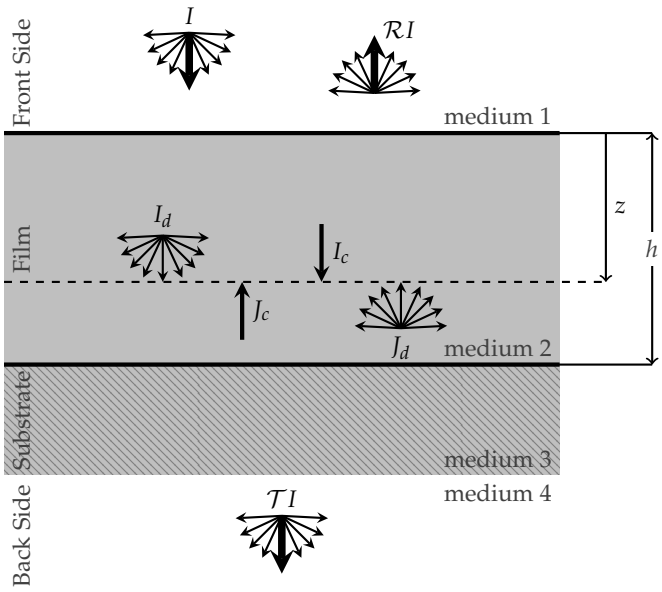

Fig. 1. Sketch of the system and the fluxes. A finitely thick plane-parallel light-scattering medium (thickness $\equiv h$) placed in optical contact with an arbitrary substrate. Incident light I, as well as the reflected ($\mathcal{R}I$) and transmitted light ($\mathcal{T}I$), are considered to be partially collimated.

Below, we provide the solution to the RTE using a four-flux model for this system when it is illuminated with partially collimated light, i.e., light that has both a collimated and a diffuse contribution. Expressions for the reflectance and transmittance in the aforementioned system are provided in [23] for the case of totally collimated incident light.

Taking into account the energy balances, the differential equations describing the system are

$$\frac{\mathrm{d}I_c}{\mathrm{d}z} = -(\alpha+\beta)I_c \quad \textbf{(1)}$$

$$\frac{\mathrm{d}J_c}{\mathrm{d}z} = (\alpha+\beta)J_c \quad \textbf{(2)}$$

$$\frac{\mathrm{d}I_d}{\mathrm{d}z} = \xi[(1-\sigma_d)\alpha(J_d-I_d)-\beta I_d]+\sigma_c\alpha I_c+(1-\sigma_c)\alpha J_c \quad \textbf{(3)}$$

$$\frac{\mathrm{d}J_d}{\mathrm{d}z} = \xi[\beta J_d+(1-\sigma_d)\alpha(J_d-I_d)]-\sigma_c\alpha J_c-(1-\sigma_c)\alpha I_c, \quad \textbf{(4)}$$

where α and β are the scattering and absorption coefficients per unit length, ξ is the average path length traveled by diffuse light as compared to collimated light, and σ_c and σ_d are the forward scattering ratio coefficients, i.e., the amount of light scattered into the forward hemisphere, for collimated and diffuse light respectively. A full derivation of the solutions for the equations is given in appendix A. Parameters involved in the four-flux model are studied in more detail in appendix B.

Following the approach used in [19] to solve equations (1) to (4) we obtain an expression of each flux as a function of z

$$I_c(z) = c_1 e^{-\zeta z} \tag{5}$$
$$J_c(z) = c_2 e^{\zeta z} \tag{6}$$
$$J_d(z) = c_3 \cosh(Az) + c_4 \sinh(Az) + c_5 e^{\zeta z} + c_6 e^{-\zeta z} \tag{7}$$
$$I_d(z) = c_7 \cosh(Az) + c_8 \sinh(Az) + c_9 e^{\zeta z} + c_{10} e^{-\zeta z}, \tag{8}$$

where only four coefficients, c_1, c_2, c_3 and c_4, are independent. The expressions for the coefficients c_i are given in appendix A. The solutions to the differential equations are expressed in terms of the following constants to be more concise

$$A = \xi \sqrt{\beta[\beta + 2\alpha(1-\sigma_d)]} \tag{9}$$
$$B = \alpha[\xi\beta\sigma_c + \xi\alpha(1-\sigma_d) + \zeta\sigma_c] \tag{10}$$
$$C = \alpha\{\xi[\alpha(1-\sigma_d) + \beta(1-\sigma_c)] - \zeta(1-\sigma_c)\} \tag{11}$$
$$D = \xi[\beta + \alpha(1-\sigma_d)] \tag{12}$$
$$E = \xi\alpha(1-\sigma_d) = D - \xi\beta, \tag{13}$$

where $\zeta = \alpha + \beta$ is the extinction coefficient per unit length.

The total light intensity at a given z can be easily evaluated from the sum of all fluxes which can be associated to the transverse energy density $\mathcal{U}(z)$

$$\mathcal{U}(z) = I_c(z) + I_d(z) + J_c(z) + J_d(z). \tag{14}$$

From equations (5) to (8), explicit expressions for the effective light transfer across the system can be obtained. The system's total reflectance and transmittance have an specular contribution ($\mathcal{R}_c$, $\mathcal{T}_c$), the light that has remained collimated, and a diffuse contribution composed of: the collimated incident light that is scattered ($\mathcal{R}_{cd}$, $\mathcal{T}_{cd}$) and the diffuse incident light ($\mathcal{R}_{dd}$, $\mathcal{T}_{dd}$). Therefore, the total reflectance and transmittance can be expressed as

$$\mathcal{R} = f\mathcal{R}_c + \mathcal{R}_d = f(\mathcal{R}_c + \mathcal{R}_{cd}) + (1-f)\mathcal{R}_{dd} \tag{15}$$
$$\mathcal{T} = f\mathcal{T}_c + \mathcal{T}_d = f(\mathcal{T}_c + \mathcal{T}_{cd}) + (1-f)\mathcal{T}_{dd}, \tag{16}$$

where f is the fraction of collimated incident light. The specular and diffuse contributions to the total reflectance are

$$\mathcal{R}_c = r_{c12} + \frac{(1-r_{c12})^2 R_{sc} e^{-2\zeta h}}{1 - r_{c12} R_{sc} e^{-2\zeta h}} \tag{17}$$
$$\mathcal{R}_{cd} = \frac{(1-r_{d21})(1-r_{c12}) e^{-\zeta h}[C_0 + C_1 e^{\zeta h} + C_2 e^{-\zeta h}]}{(A^2-\zeta^2)(1-r_{c12}R_{sc}e^{-2\zeta h})DEN} \tag{18}$$
$$\mathcal{R}_{dd} = r_{d12} - \frac{(1-r_{d21})(1-r_{d12})}{DEN} \times [AR_{sd}\cosh(Ah) + (E - R_{sd}D)\sinh(Ah)], \tag{19}$$

and the contributions to the transmittance are

$$\mathcal{T}_c = \frac{(1-r_{c23})(1-r_{c34})\tau_c(1-r_{c12})e^{-\zeta h}}{(1-r_{c23}r_{c34}\tau_c^2)(1-r_{c12}R_{sc}e^{-2\zeta h})} \tag{20}$$
$$\mathcal{T}_{cd} = \left[(1-r_{c12})(1-r_{d23})(1-r_{d34})\tau_d e^{-\zeta h}\right] \times \frac{D_1\cosh(Ah) + D_2\sinh(Ah) + D_3 e^{\zeta h} + D_4 e^{-\zeta h}}{(1-r_{d32}r_{d34}\tau_d^2)(1-r_{c12}R_{sc}e^{-\zeta h})(A^2-\zeta^2)DEN} \tag{21}$$
$$\mathcal{T}_{dd} = -\frac{(1-r_{d12})(1-r_{d23})(1-r_{d34})A\tau_d}{(1-r_{d32}r_{d34}\tau_d^2)DEN}, \tag{22}$$

where r_{cij} and r_{dij} are the reflectance factors for collimated and diffuse light at the interface between media i and j as indicated in figure 1. The factors greatly depend upon whether the diffuse flux is incident toward positive or negative z. Expressions for evaluating the reflectance factors from media's refractive indices are given in appendix B. DEN is given by

$$DEN = A(R_{sd}r_{d21} - 1)\cosh(Ah) + [E(R_{sd} + r_{d21}) - D(1 + r_{d21}R_{sd})]\sinh(Ah), \tag{23}$$

coefficients C_i and D_i are given in appendix A and the multiple boundary reflections at the substrate are taken into account in R_{sc} and R_{sd}, the effective reflection coefficients for collimated and diffuse radiation at the film-substrate interface,

$$R_{sc} = \frac{r_{c23}(1 - 2r_{c34}\tau_c^2) + r_{c34}\tau_c^2}{1 - r_{c23}r_{c34}\tau_c^2}, \tag{24}$$
$$R_{sd} = \frac{r_{d23} + (1 - r_{d23} - r_{d32})r_{d34}\tau_d^2}{1 - r_{d32}r_{d34}\tau_d^2}, \tag{25}$$

where τ_c and τ_d are the internal transmittance coefficients, i.e., the fraction of light that traverses the substrate without being absorbed, for collimated and diffuse light respectively.

It is worth noting that the expressions from [23] are recovered if we illuminate the system with totally collimated light ($f = 1$).

In this work, we derive new expressions to evaluate the substrate's contribution to the total absorptance and therefore, a method to evaluate the different absorptance contributions. The system's total absorptance is simply the amount of light that is neither reflected nor transmitted. Mathematically is given by

$$\mathcal{A} = 1 - \mathcal{R} - \mathcal{T}. \tag{26}$$

Light can only be absorbed at either the film or the substrate. Thus, $\mathcal{A}$ can be rewritten as a sum of the light absorbed within the film $\mathcal{A}_f$ and within the substrate $\mathcal{A}_s$

$$\mathcal{A} = \mathcal{A}_f + \mathcal{A}_s = \mathcal{A}_f + f\mathcal{A}_{sc} + (1-f)\mathcal{A}_{sd}, \tag{27}$$

where the specular, A_{sc}, and the diffuse, A_{sd}, contributions to $\mathcal{A}_s$ are given by

$$\mathcal{A}_{sc} = \frac{(1-r_{c12})[D_1\cosh(Ah) + D_2\sinh(Ah) + D_3 e^{\zeta h} + D_4 e^{-\zeta h}]}{(1-r_{c12}R_{sc}e^{-2\zeta h})(A^2-\zeta^2)DEN} + \frac{[(1-r_{c23})(1-\tau_c) + r_{c31}\tau_c(1-\tau_c-r_{c23}+r_{c23}\tau_c)](1-r_{c12}e^{-\zeta h})}{(1-r_{c23}r_{c34}\tau_c^2)(1-r_{c12}R_{sc}e^{-2\zeta h})} \tag{28}$$
$$\mathcal{A}_{sd} = -\frac{[(1-r_{d23})(1-\tau_d) + r_{d34}\tau_d(1-\tau_d-r_{d23}\tau_d)](1-r_{d12})A}{(1-r_{d32}r_{d34}\tau_d^2)DEN}. \tag{29}$$

A derivation of equations (28) and (29) is provided at appendix A.

A. Kubelka-Munk Limit

The KM model can be understood as a limiting case of the four-flux model in which the system is shined on with only perfectly diffuse light. Therefore, applying the conditions necessary to satisfy the assumptions made in the KM model, we can retrieve the KM expressions. This comparison is conducted as a cross-check of the equations' derivation.

In the KM limit, the incident light is completely diffuse ($f = 0$) and only the film and the substrate are considered,

Table 1. Probabilities correspondence. Correspondence between the different probabilities considered in our MC approach and the physical parameters of the four-flux theory.

Probability	Physical parameter	Description
PK^{col}	$\beta\,\mathrm{d}z$	Absorption probability for a collimated beam
PK^{dif}	$\xi\beta\,\mathrm{d}z$	Absorption probability for a diffuse beam
PR^{col}	r_{cij}	(Fresnel) Reflection probability for a collimated beam
PR^{dif}	r_{dij}	(Fresnel) Reflection probability for a diffuse beam
$PS^{\text{col}}_{\text{back}}$	$\alpha(1-\sigma_c)\,\mathrm{d}z$	Backscattering probability for a collimated beam
$PS^{\text{dif}}_{\text{back}}$	$\xi\alpha(1-\sigma_d)\,\mathrm{d}z$	Backscattering probability for a diffuse beam
$PS^{\text{col}}_{\text{forward}}$	$\alpha\sigma_c\,\mathrm{d}z$	Forward scattering probability for a collimated beam

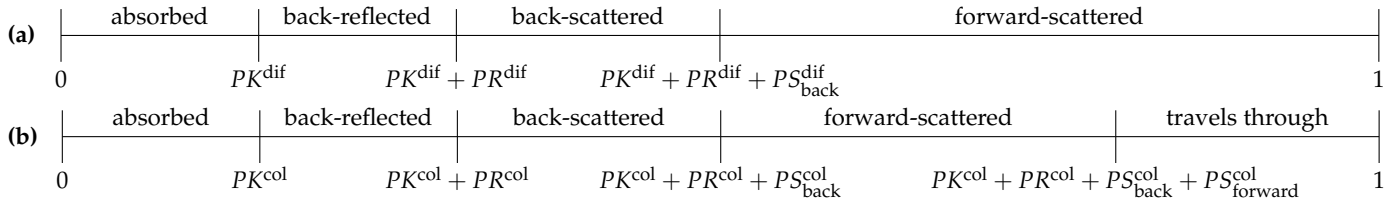

Fig. 2. Probability *allocation* for: **(a)** a diffuse beam and **(b)** a collimated beam.

which implies that $r_{d12} = r_{d21} = r_{d31} = 0$. Using the following relationships between the KM coefficients and ours

$$R_g = r_{d23} = R_{sd} \qquad A = \sqrt{K^2 + 2KS} = Sb$$
$$T_g = (1 - r_{d23})\tau_d \qquad D = \sqrt{K + S}$$
$$K = \xi\beta \qquad E = S$$
$$S = \xi\alpha(1-\sigma_d) \qquad X = h,$$

where R_g and T_g are the reflectance and transmittance of the substrate, X is the thickness of the film, K and S are the KM absorption and backscattering coefficients, $b = \sqrt{a^2 - 1}$ and $a = 1 + K/S$, the KM expressions given in [14] are then recovered.

3. MONTE CARLO APPROACH

In order to simulate the four-flux theoretical model described in figure 1, we implement a MC approach. Specifically, we discretize the film in N_l layers and couple it to additional layers that account for: reflections at the different interfaces (air-film, film-substrate, substrate and substrate-air), and the absorption at the substrate. We assign absorption, reflection and scattering probabilities to each layer (including the substrate).

Table 1 shows the correspondence between the different probabilities considered in our MC approach and the physical parameters of the four-flux theory.

Figure 2 shows the probability *allocation* for diffuse and collimated beams, respectively. We send N_T elemental light beams to the specimen and decide their fate according to algorithm 1.

Algorithm 1 Four-flux Monte Carlo.

▷ Each incoming beam is initially moving to the right
while moving **do**
  $\rho \leftarrow$ uniformly distributed random number $\in (0, 1)$
  if collimated **then**
    if $\rho < PK^{\text{col}}$ **then** ▷ beam absorbed
      beam absorbed
      STOP
    else if $\rho < (PK^{\text{col}} + PR)$ **then** ▷ beam back-reflected
      if moving to the right **then**
        if first layer **then**
          beam reflected (specular)
          STOP
        else
          reverse direction
          back one layer
      else
        reverse direction
        move one layer
    else if $\rho < (PK^{\text{col}} + PR + PS^{\text{col}}_{\text{back}})$ **then** ▷ beam back-scattered
      if moving to the right **then**
        if first layer **then**
          beam reflected (diffuse)
          STOP
        else
          reverse direction
          back one layer
          collimated = false
      else
        reverse direction
        move one layer
        collimated = false
    else if $\rho < (PK^{\text{col}} + PR + PS^{\text{col}}_{\text{back}} + PS^{\text{col}}_{\text{forward}})$ **then** ▷ beam forward-scattered
      if moving to the right **then**
        if last layer **then**
          beam transmitted (diffuse)
          STOP
        else
          move one layer

```
                collimated = false
            else
                if first layer then
                    beam reflected (diffuse)
                    STOP
                else
                    back one layer
                    collimated = false
        else                                ▷ beam travels through
            if moving to the right then
                if last layer then
                    beam transmitted (specular)
                    STOP
                else
                    move one layer
            else
                if first layer then
                    beam reflected (specular)
                    STOP
                else
                    back one layer
    else
        Algorithm 1: Monte Carlo approach algorithm [14]
```

The MC simulation model outputs the total number of reflected, transmitted and absorbed beams, the total number of beams hitting a given layer (associated to the transverse energy density $\mathcal{U}(z)$) and the total number of time units, a time unit is defined as the time that a collimated beam takes to cross of a layer of the vacuum, i.e., $n = 1$, of each beam before being either reflected, transmitted or absorbed, which may be associated to its time-of-flight (ToF).

As it will be shown, the total number of incoming beams, N_T, determines the precision of the calculation, or the statistical uncertainty, i.e., the difference between consecutive realizations under the same simulation conditions. On the other hand, the accuracy of the calculation, i.e., the difference between the real and the simulated values, depends on the total number of layers, N_l. Given that the total probability for a beam to be scattered (absorbed) within the medium αh (βh) must be equal to the N_l times the layers' probability for scattering (absorption), N_l can be defined as

$$N_l = \frac{(\xi+1)\zeta h - \xi\alpha\sigma_d h}{\sum_i P_i}, \tag{30}$$

where

$$\sum_i P_i = PK^{\text{col}} + PK^{\text{dif}} + PS^{\text{col}}_{\text{back}} + PS^{\text{dif}}_{\text{back}} + PS^{\text{col}}_{\text{forward}}. \tag{31}$$

It should be noted that the total event probability for a collimated (diffuse) photon is only $PK^{\text{col}} + PS^{\text{col}}_{\text{back}} + PS^{\text{col}}_{\text{forward}}$ ($PK^{\text{dif}} + PS^{\text{dif}}_{\text{back}}$) which is always $\leq \sum_i P_i$. Therefore the criterion given in equation (31) is even more restrictive. The total event probability for each layer, $\sum_i P_i$, directly determines the number of layers needed to correctly describe the physical phenomena taking place, and reproduce the theoretical results. Apart from the obvious probability limit $\sum_i P_i \leq 1$, a convergence criterion must be established. As our MC model implements the same assumptions as the four-flux theory described in section 2, for a first verification we compare simulated and theoretical results of the collimated and diffuse reflectance, $\mathcal{R}_c$ and $\mathcal{R}_d$, and transmittance, $\mathcal{T}_c$ and $\mathcal{T}_d$. Figure 3 shows the difference (in percentage points) between simulated and theoretical results of $\mathcal{T}_c$ as a function of the number of layers and $\sum_i P_i$. Similar results are obtained for the other magnitudes.

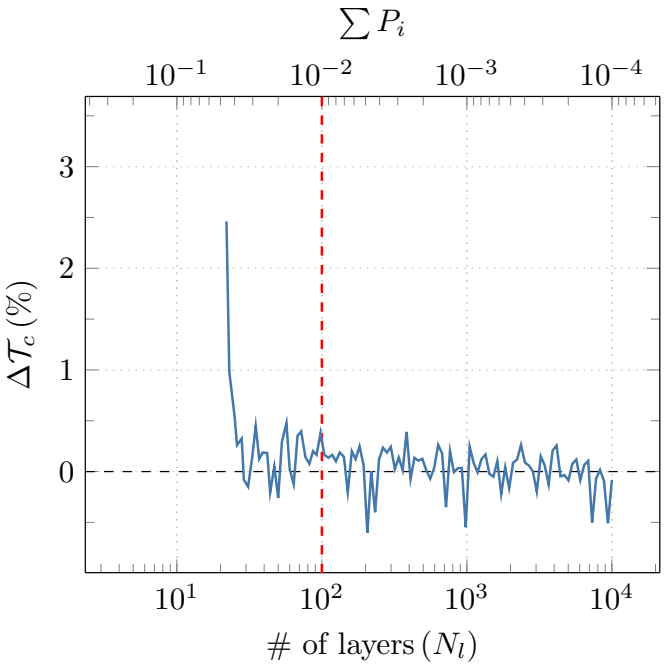

Fig. 3. Absolute difference (in percentage points) between simulated and theoretical results of the collimated transmittance, as a function of N_l and $\sum_i P_i$ (top axis). Parameters: $\alpha = 0.4$ mm^{-1}, $\beta = (1-2\alpha)/3$ mm^{-1}, $h = 1$ mm, $n_1 = n_3 = n_4 = 1.0$, $n_2 = 1.8$, $\tau_c = 1$, $f = 0.5$.

As can be seen in figure 3, for $\sum_i P_i = 0.01$ the absolute difference between simulated and exact results is already stabilized, so that we take

$$\sum_i P_i \leq 0.01 \tag{32}$$

as a discretization criterion. As a means to visualize the effect of both N_l and N_T on the accuracy and precision of the calculations in a typical case, we set $\alpha = 0.5$ mm^{-1}, $\beta = 0.05$ mm^{-1}, $h = 1$ mm, $n_1 = n_4 = 1.0$, $n_2 = 1.5$, $n_3 = 1.0$, $\sigma_c = 0.5$, $\sigma_d = 0.5$, $\xi = 2$, $\tau_c = 1$, $\tau_d = \tau_c^2$, $f = 1.0$ and calculate $\mathcal{R}_c$, $\mathcal{R}_d$, $\mathcal{T}_c$ and $\mathcal{T}_d$ for several levels of discretization (growing N_T, progressively lower $\sum_i P_i$), as a function of ζh, the net extinction within the medium. For each discretization, 100 realizations were carried out, calculating an average value together with the associated standard deviation. This is shown in figure 4, with markers showing the average value and error bars representing $\pm$ standard deviation.

As expected, simulated results converge (with an excellent agreement) to theoretical ones as N_T is increased and $\sum_i P_i$ is decreased, i.e., discretization layers are made thinner for the same specimen. Interestingly, as $\sum_i P_i$ decreases we achieve more accuracy (average value approaches zero) while increasing N_T reduces the overall noise associated with the random number generation (see the length of the error bars in figure 4). Moreover, we observe that when the criterion established in equation (31) is satisfied the differences between the theoretical and simulated results are compatible to being null as expected.

According to these results, if not stated otherwise, from now on all MC simulations are performed sending 100 000 elemental

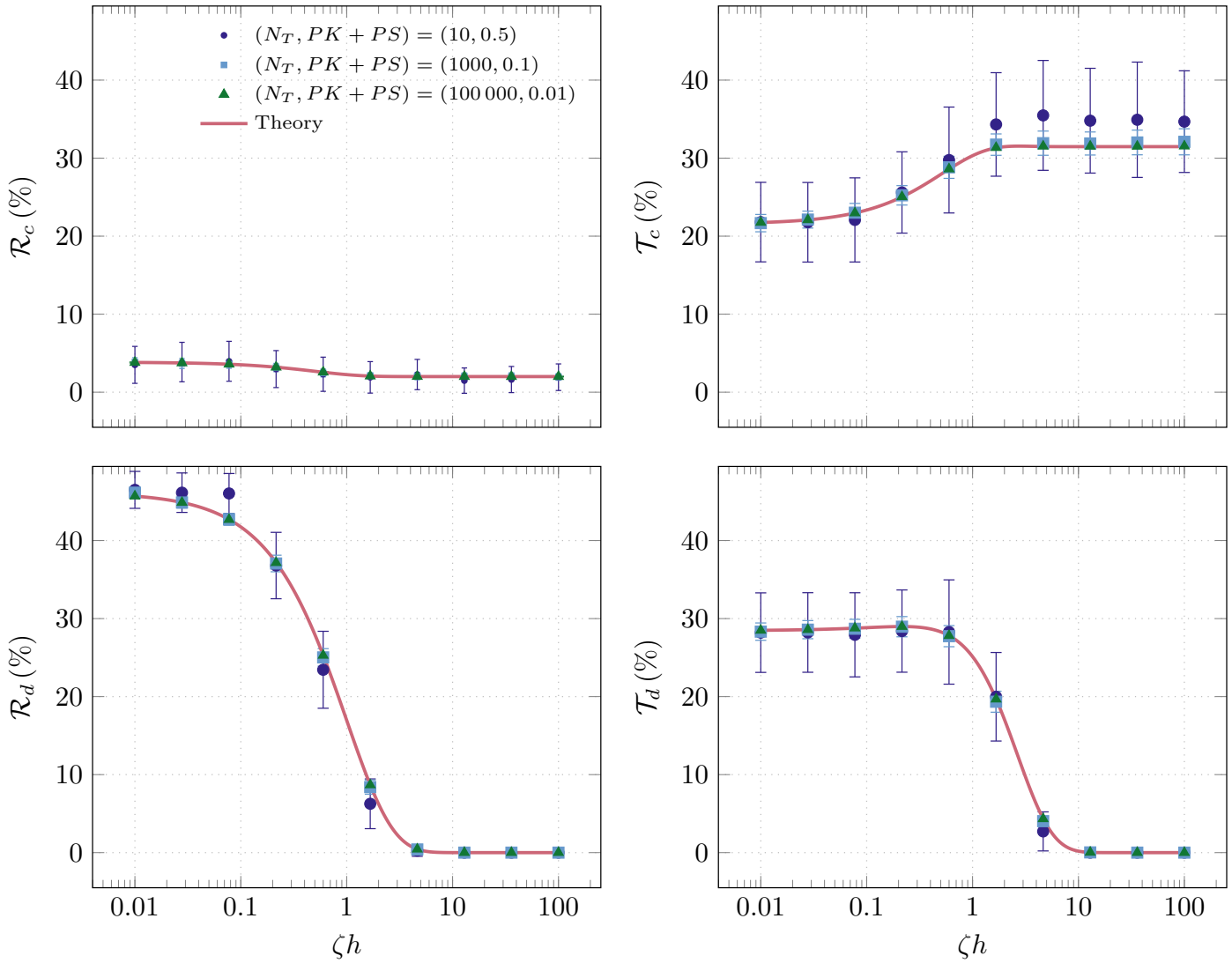

Fig. 4. Theoretical and simulated values comparison of $\mathcal{R}_c$, $\mathcal{R}_d$, $\mathcal{T}_c$ and $\mathcal{T}_d$ as a function of the thickness with increasing extinction ($\zeta = \alpha + \beta$ with $\alpha = 10\beta$) for different discretizations, i.e., different $\sum_i P_i$, and number of beams (NT). Parameters: $h = 1$ mm, $n_1 = n_3 = n_4 = 1.0$, $n_2 = 1.5$, $\tau_c = 1$, $f = 0.5$.

beams to a specimen discretized with a number of layers so that equation (32) is fulfilled.

4. RESULTS

Among the many results that can be obtained with this MC we have focused on some with practical interest. In section A we have examined the transverse energy density within the film at equilibrium. The single scattering penetration depth, a parameter that provides information about how fast collimated light is scattered, is studied in section B. We have analyzed the absorptance contributions for different substrates section C. And, last but not least, the temporal distribution of an ultra-short pulse is studied in section D.

A. Transverse energy density

The theoretical transverse energy density at a given depth can be related to the number of total beams hitting a layer at that specific depth. Figure 5 shows a comparison between the theoretical and simulated results of the transverse energy density relative to I, the total incident intensity, as a function of the relative film's depth for several values of the ratio β/α, i.e., the ratio between the absorption and the scattering.

The results shown are valid only under a constant incident radiation. If the incident ration is time-dependent, i.e., $I \equiv I(t)$, the transverse energy density will not be generally constant over time. Unlike the MC, analytical solutions of the four flux model only provide information when the fluxes are at equilibrium with the incident radiation. We show in section D an application of the MC when the system is shined on with a time-dependent radiation, in particular a collimated pulse of light.

The agreement between theory and simulation shown in figure 5 is excellent. Moreover, the transverse energy density decreases more rapidly in more absorbing media, as expected from propagating beams.

We also observe that when the absorption is not negligible the transverse energy density has an exponential decay as in a Beer-Lambert case. When the scattering contribution is larger than the absorption contribution, U is larger at smaller z. Increasing

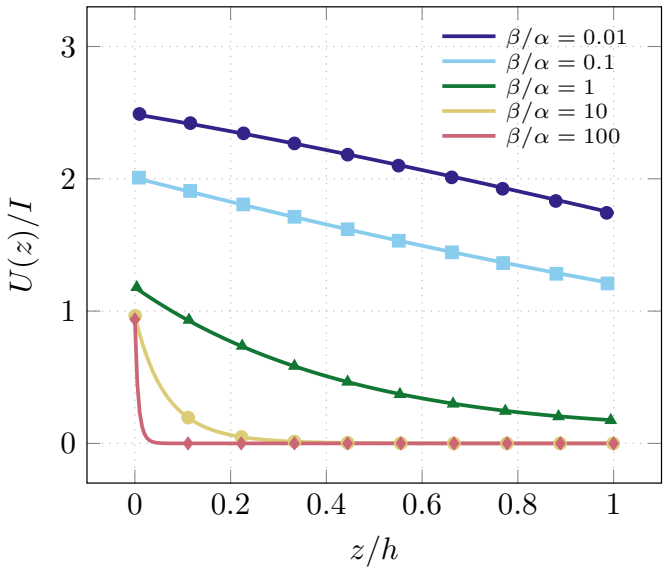

Fig. 5. Transverse energy density relative to the initial intensity I as a function of the medium's depth for different values of the β/α ratio. The solid lines (markers) show the theoretical (simulated) results. Parameters: $\alpha = 1\ \mathrm{mm}^{-1}$, $h = 1$ mm, $n_1 = n_4 = 1.0$, $n_2 = 1.5$, $n_3 = 1.0$, $\tau_c = 1$, $f = 0.5$.

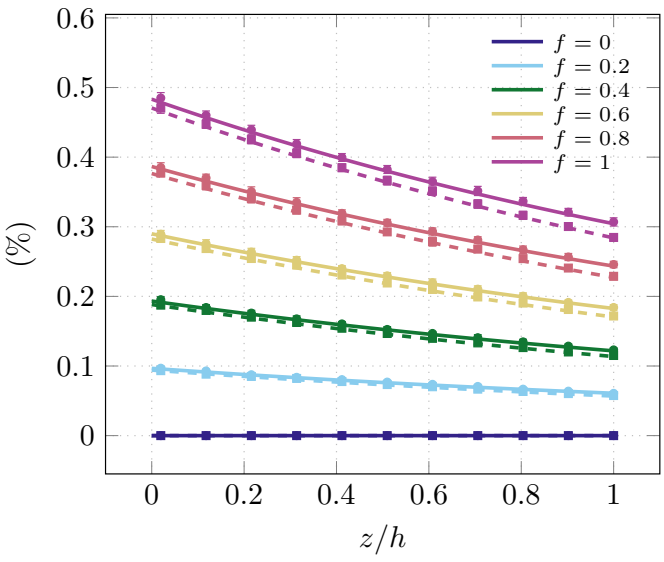

Fig. 6. Simulated (markers) and theoretical (solid lines) percentage of beams that have become diffuse at a given medium's depth for different fractions of the initially collimated beams when reflections at the interface tissue/substrate are taken into account (solid lines) and when they are not (dotted lines). Parameters: $\alpha = 0.5\ \mathrm{mm}^{-1}$, $\beta = 0.005\ \mathrm{mm}^{-1}$, $h = 1$ mm, $n_1 = 1.0$, $n_2 = 1.41$ (refractive index of a mammal tissue [32]), $\tau_c = 1.0$ and, $n_3 = 1.5$, $n_4 = 1$ for the first and $n_3 = n_4 = 1.41$ second case respectively, $N_T = 10^6$ beams.

the scattering increases the number of direction changes that light beams experience. This results in a concentration raise of light beams near the first media interface which results in an increase in diffuse reflectance and a decrease in the number of photons that cross the medium.

It is worth noting that the ratio $\mathcal{U}$ to I can be larger, and indeed it is for highly scattering media, i.e., $\alpha \gg$, than unity. This is a typical result of a system in which light travels back and forth, e.g., passive optical cavity.

B. Single scattering penetration depth

Another result from the MC that can be verified with theory is the number of collimated beams that have experienced scattering at a given layer. The amount of collimated light that has undergone scattering between z and $z + \mathrm{d}z$ is equal to the collimated intensity, i.e., the sum of the collimated fluxes, at z multiplied by the probability of being scattered in a $\mathrm{d}z$. Thus, for a given discretization, the scattered collimated intensity is

$$\begin{aligned} I_s(z) =& I_c(z) + J_c(z) \\ =& \left(\frac{\alpha h}{N}\right) \frac{(1 - r_{c12}) f I}{1 - r_{c12} R_{sc} e^{-2\zeta h}} [e^{-\zeta z} + R_{sc} e^{-2\zeta h} e^{\zeta z}], \end{aligned} \tag{33}$$

where we have used equation (5) and equation (6).

From equation (33) the single scattering penetration depth, i.e., the depth at which the intensity of the collimated radiation inside the material falls to $1/e$, can be evaluated. This magnitude has a potential importance in tissue spectroscopy. Light rays that undergone scattering in a biological sample can suffer single or multiple scattering. Single scattered light arise predominantly from the scattering at the tissue surface. On the other hand, light that experiences more scattering events within the tissue contains information about deeper scattering structures [31].

Here, we study the depth at which single scattering occurs in two cases, first a film over a non-absorbing substrate and second a free-standing film. Thus, reflections at the film/substrate interface are only taken into account in the former case, i.e., the second term in equation (33) is zero in the latter. These systems are a simple model of a tissue on a sample holder and a free-standing tissue. Figure 6 presents theoretical and simulated values of the percentage of collimated beams that have become diffuse, i.e., that has undergone single scattering, in a width h/N at a given depth z.

We observe that the number of scattered beams decreases with increasing depth and decreasing f since there are less beams subject to be scattered. Reflections at the substrate yield to an overall increase of the beams scattered within the medium. The longer they are in the medium the higher the probability for experiencing scattering. Unsurprisingly, the largest difference occurs at the largest z, in other words, when light is closest to the film/substrate interface.

C. Absorption contributions

The MC enables us to tell apart between light absorbed at the film from light absorbed at the substrate. Here we try to show the strength of the substrate's contribution to the total absorptance. We have evaluated the amount of light absorbed at both the film and the substrate with increasing probability for light to be absorbed within the film (βh). Figure 7 compares the simulated results and theoretical results of the absorptances. Two cases have been considered, one in which the absorption at the substrate is large, figure 7 a), and other in which it is low, figure 7 b).

It is observed in figure 7 that the agreement between theory and simulation is splendid. Moreover, the film's absorption contribution grows with the probability of being absorbed at the film as expected. When $\beta h \geq 1$, all light entering the system is absorbed and is absorbed at the film. When the $\beta h \ll 1$ the

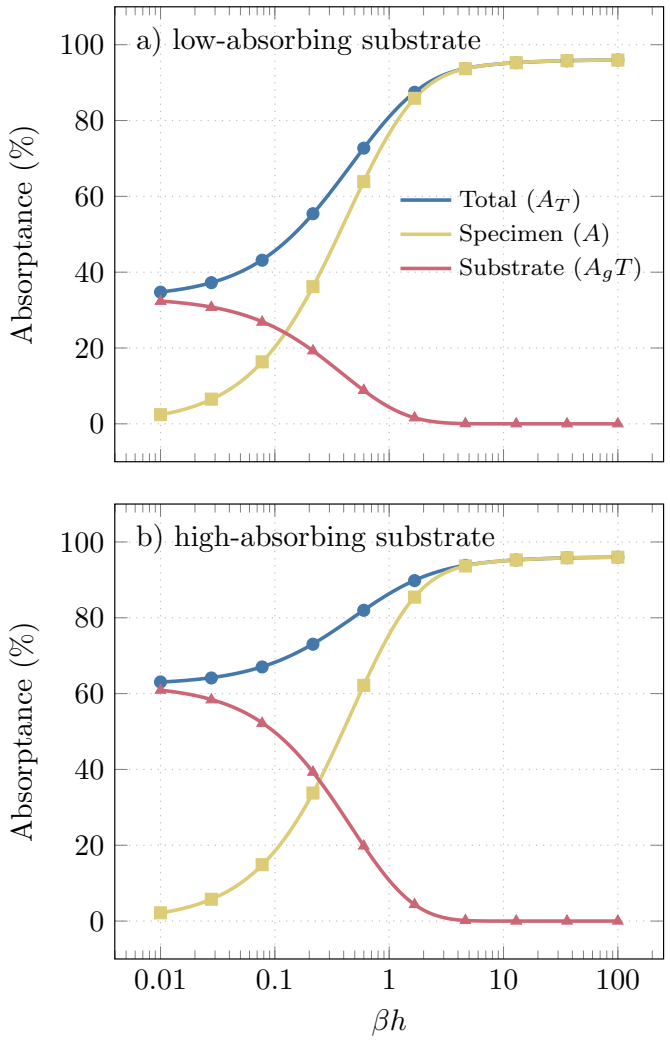

Fig. 7. Theoretical (solid lines) and simulated (markers) results of the total absorptance $\mathcal{A}$ as well as the film's $\mathcal{A}_f$ and substrate's $\mathcal{A}_s$ contribution to the absorptance for a low-absorbing substrate, show in the figure at the top ($\tau_c = 0.8$), and for a high-absorbing substrate, figure at the bottom ($\tau_c = 0.2$). Parameters: $\alpha = 1\text{mm}^{-1}$, $h = 1\text{mm}$, $n_1 = n_4 = 1.0$, $n_2 = 1.3$, $n_3 = 1.5$, $f = 0.5$.

light absorption occurs mainly within the substrate and as βh this contribution decreases since less light reaches the substrate.

D. Time-of-Flight (ToF)

MC also tracks the ToF of each beam, i.e., the number of time units elapsed by each beam before it is either reflected, transmitted or absorbed. This magnitude provides useful information that it is not available analytically, e.g., the temporal distribution of a pulse of light or, equivalently, the transient state of the magnitudes $\mathcal{R}_c$, $\mathcal{T}_c$, etc.

As an illustrative example we have studied the temporal distribution of an ultra-short collimated pulse incident on a heterogeneous system composed of two layers of different translucent media over a substrate. The system under consideration is equivalent to the system shown in figure 1 with the exception of the film being constituted by two different media. In table 2 the physical properties of the system studied are shown. The layer closest to the substrate has a larger scattering and absorption contribution than the other. This system can represent the case of a sequence of two different coatings applied to a transparent substrate. The system of layers is embedded in air. The pulse can be modeled as a $\delta(t = 0)$ by sending a bunch of N_T beams at a specific time.

Table 2. System's properties. Physical properties of the two coatings ($i = 1, 2$), and the substrate ($i = 3$) of the system understudy. n is the refractive index, α (β) is the scattering (absorption) coefficient per unit length, h is the width of the layer, and l is the number of layers in which the corresponding medium has been discretized.

i	n	$\alpha\ \left(\text{mm}^{-1}\right)$	$\beta\ \left(\text{mm}^{-1}\right)$	h (mm)	l
1	1.5	0.1	0.1	1	502
2	1.8	1	1	1	502
3	1.5	0	0	2	1004

Let the time that a collimated beam takes to cross a layer of a medium with refractive index $n = 1$, i.e., in vacuum, be a time element Δt. Under uniform discretization, the time elapsed by a collimated (diffuse) beam to go through a layer with refractive index n is $t_c = n\Delta t$ ($t_d = \xi n\Delta t$). The temporal distribution of a collimated pulse incident on the system is shown in figure 8.

For a delta function-like pulse, the collimated magnitudes take non-zero values at specific times while the diffuse magnitudes are spread over time. This is a result of collimated beams traveling all together as a ballistic bunch, being susceptible of exiting the system only when it reaches the system's edges. The perturbation within the system due to the pulse decreases as beams are either reflected, transmitted or absorbed. Thus, we observe in figure 8 that the (%) of beams decreases with increasing time.

Let us analyze each magnitude individually. Regarding the collimated reflectance (blue bars in figure 8, top), the first peak ($t = 0$) corresponds to light that is reflected at the first interface. The second contribution ($t = 2n_1l_1 \simeq 1506$) is due to light that crosses the first medium, suffers a reflection at the interface between the media and exits the system from the first interface. The third ($t = 4n_1l_1 \simeq 3013$) comes from the small amount of beams that suffers several reflections at the following interfaces: medium 1-medium 2, medium 1-air and medium 1-medium 2. The fourth peak ($t = 2(n_1l_1 + n_2l_2) \simeq 3317$) arises due to light that is reflected at the medium 2-substrate interface. The following peaks can be understood using similar arguments. Analogously, if we analyze the collimated transmittance's peaks (orange bars in figure 8, top) we see that the first one ($t = n_1l_1 + n_2l_2 + n_sl_s \simeq 3163$) corresponds to light that crosses the whole system and goes through the last interface. The second peak is light that reflects at the interface medium 1-medium 2, reflects back at the interface air-medium 1 and leaves the system from the back side ($t = 2n_1l_1 + n_2l_2 + n_sl_s \simeq 4669$), etc.

In the case of diffuse reflectance we can see a continuous contribution from light that enters the system, suffers multiple scattering eventually turning around exiting the system at the first interface. We also observe periodical enhancements. The enhancements occur when the ballistic bunch reaches the first interface. New diffuse beams coming from the scattering of the collimated bunch add to the continuous background of diffuse

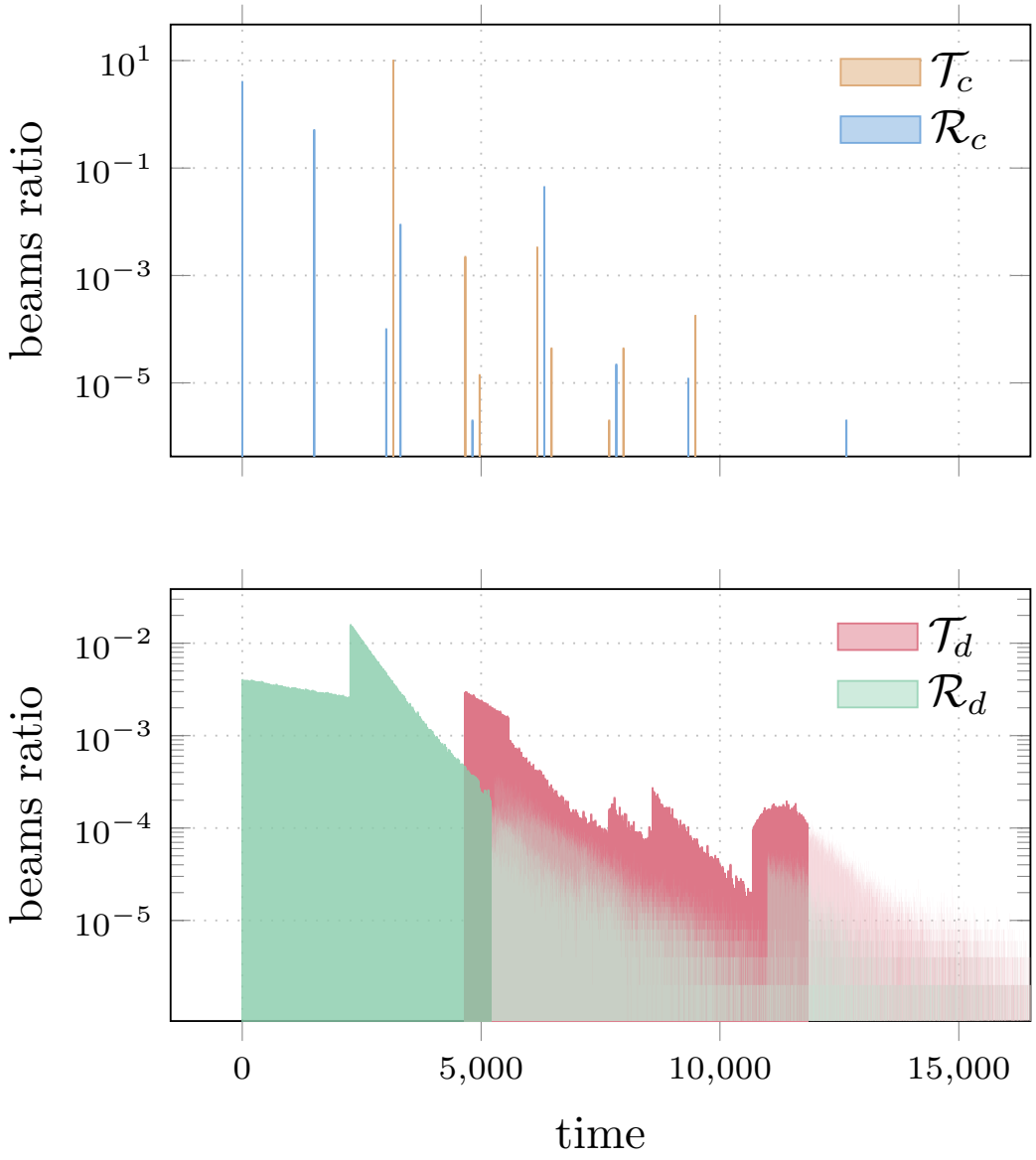

Fig. 8. Response function of the system to a delta-like pulse. Histogram showing the ratio of collimated and diffuse beams that have been either reflected or transmitted as a function of time. The bin width is equal to a time element Δt. The total number of incident beams utilized in this simulation is: $N_T = 5 \times 10^7$.

beams yielding an increase in the diffuse reflectance. With regard to the diffuse transmittance, it starts at $t = n_1 l_1 + n_2(l_2 - 1) + 2(n_2 + n_s l_s) \simeq 4670$, i.e., light that has remained collimated until experiencing scattering at the end of the medium 2 layer. Note that, in this case, the last scattering layer does not coincide with the last layer of the system. It behaves like the diffuse reflectance with the exception that the enhancements occur when the ballistic bunch arrives at the last interface.

From figure 8 it is evident that there is a time delay between the first collimated and diffuse transmitted beams. The first outgoing collimated beam is found at $t \simeq 3163$, while the first diffuse beam do it at $t \simeq 4670$. This artificial difference arises due to the fact that all the diffuse beams are set to cross the same distance as collimated beams in double the time, i.e., taking the average pathlength $\xi = 2$ for all diffuse beams instead of taking random values with a mean value of $\xi = 2$ for each beam.

Note that all collimated transmitted pulses but the first one, will be overlapped with the transmitted diffuse contribution since they have similar intensities. On the other hand, there are several collimated reflected pulses with a significantly larger intensity than the reflected diffuse contribution even at time over $6000\Delta t$.

Figure 8 shows the system's impulse-response function. Therefore, the system's response to a pulse described by a general function of time ($f \equiv f(t)$) is simply the convolution of the pulse's function and the system's impulse-response function. While a time unit in our system is on the order of $\Delta t = h/(cl) \simeq 7$ fs, a more realistic pulse would have a time spread of 100 fs. In this particular case, we still would be able to distinguish reflected and transmitted peaks, since the time differences between the maxima of the peaks are larger than the peaks' time spread.

5. CONCLUSIONS

We have reviewed the four-flux model applied to an homogeneous slab with scattering inclusions located on top of an absorbing substrate under partially collimated incident light. We have also calculated the transverse energy density in the slab and the different contributions to the total absorptance. We have also recovered the KM expressions in the limit of perfectly diffuse incident light.

Moreover, a MC algorithm to simulate the four-flux model has been implemented. In the MC approach the medium is discretized in layers each of them characterized by the probability of light undergoing reflection, absorption or scattering. We have derived a correspondence between the physical parameters involved in the four-flux model and the probabilities of the layers. A comparison between the MC results and the four-flux model predictions enabled us to cross-check the validity of the expressions and the MC itself.

The MC approach has an added value, as it allows, among other things, for the implementation of inhomogeneities in the specimen itself or the treatment of nonlinear phenomena. It also incorporates time, which finds application in the study of light pulses as it has been shown in section D. Transient states could also be studied in the framework of N-flux models by solving equations (1) to (4) using standard numerical methods for solving ODEs, such as Runge-Kutta. However, the Monte Carlo has advantages with respect to other numerical methods. In the first place, Monte Carlo is a very intuitive method. In the case of complex systems, ODE require more boundary conditions, while for MC just deals with probabilities. Furthermore, in the case of complex systems, such as very inhomogeneous media, convergence and computational time could be an issue for ODE solvers. Meanwhile, for MC it would be effectively the same problem for each light beam with, perhaps, the exception of requiring a larger N_T in order to decrease the overall noise.

Approximations to the RTE like N-flux models or numerical simulations are commonly used in general transport problems. A disadvantage of most numerical methods is that the correspondence with the physical properties of the system is not straightforward. We have successfully avoided that problem in the present work.

The work presented here provides a solid frame to model other systems and specific conditions. Prospective implementations include polarization effects (with possible Fabry-Perot interferences), anisotropies, fluorescence, structured materials, color effects, rough surfaces, etc. These will only be applicable as long as the infinite lateral extension approximation inherent to the N-flux model is satisfied. Otherwise, other RTE formalisms will be necessary.

FUNDING

This research has been supported by SODERCAN (Sociedad para el Desarrollo de Cantabria) and Research Vicerrectorate of the University of Cantabria through project 14JU2864661.

ACKNOWLEDGEMENT

E. H. wants to thank Ministerio de Educación, Cúltura y Deporte for her grant.

A. EQUATIONS FULL DERIVATION

In this appendix we provide a detailed derivation of the equations shown in section 2.

Differential equations solution

The solutions to equations (1) and (2) are easily obtained by direct integration and are given in equations (5) and (6). In order to solve equations (3) and (4), they first need to be decoupled. Following [19], we compute the derivative of the sum and subtraction of equations (3) and (4)

$$\begin{aligned}\frac{\mathrm{d}^2(J_d+I_d)}{\mathrm{d}z^2} &= \xi^2\beta[\beta+2(1-\sigma_d)\alpha](J_d+I_d)\\ &\quad-\xi[\beta+2(1-\sigma_d)\alpha]\alpha(J_c+I_c)\\ &\quad+(1-2\sigma_c)\alpha\zeta(J_c+I_c)\end{aligned} \tag{34}$$

$$\begin{aligned}\frac{\mathrm{d}^2(J_d-I_d)}{\mathrm{d}z^2} &= \xi^2\beta[\beta+2(1-\sigma_d)\alpha](J_d+I_d)\\ &\quad+\xi\beta(1-2\sigma_c)\alpha(J_c-I_c)\\ &\quad-\alpha\zeta[J_c-I_c].\end{aligned} \tag{35}$$

Adding and subtracting equations (34) and (35) and substituting equations (5) and (6) we obtain second order decoupled differential equations

$$-\frac{\mathrm{d}^2J_d}{\mathrm{d}z^2}+A^2J_d = Bc_2\mathrm{e}^{\zeta z}+Cc_1\mathrm{e}^{-\zeta z} \tag{36}$$

$$-\frac{\mathrm{d}^2I_d}{\mathrm{d}z^2}+A^2I_d = Cc_2\mathrm{e}^{\zeta z}+Bc_1\mathrm{e}^{-\zeta z}\,. \tag{37}$$

Applying standard procedures to solve differential equations we obtain equations (7) and (8), where the following relationships hold

$$c_5 = \frac{Bc_2}{A^2-\zeta^2} \tag{38}$$

$$c_6 = \frac{Cc_1}{A^2-\zeta^2} \tag{39}$$

$$c_9 = \frac{Cc_2}{A^2-\zeta^2} \tag{40}$$

$$c_{10} = \frac{Bc_1}{A^2-\zeta^2} \tag{41}$$

Initially there are four first order differential equations hence only four c_i coefficients are independent. We can derive expressions for c_7 and c_8 in terms of c_3 and c_4. First, we substitute equations (5) to (8) in equation (4) and regroup

$$\begin{aligned}0 &= \sinh(Az)[\xi(\beta+\alpha(1-\sigma_d))c_4+\xi(1-\sigma_d)\alpha c_8-Ac_3]\\ &\quad+\cosh(Az)[\xi(\beta+\alpha(1-\sigma_d))c_3+\xi(1-\sigma_d)\alpha c_7-Ac_4]\\ &\quad+\mathrm{e}^{\zeta z}[\xi(\beta+\alpha(1-\sigma_d))c_5+\xi(1-\sigma_d)\alpha c_9-\sigma_c\alpha c_2-\zeta c_5]\\ &\quad+\mathrm{e}^{-\zeta z}[\xi(\beta+\alpha(1-\sigma_d))c_6+\xi(1-\sigma_d)\alpha c_{10}-(1-\sigma_c)\alpha c_1-\zeta c_6].\end{aligned}$$

Isolating c_7 and c_8 from the first two terms:

$$c_7 = \frac{Dc_3-Ac_4}{E} \tag{42}$$

$$c_8 = \frac{Dc_4-Ac_3}{E}\,. \tag{43}$$

To find exact solutions we use the boundary conditions. The boundary conditions at the interface $z=0$ are

$$I_c(0) = (1-r_{c12})fI+r_{c12}J_c(0) \tag{44}$$

$$I_d(0) = (1-r_{d12})(1-f)I-r_{d21}J_d(0), \tag{45}$$

where I is the incident light intensity. The boundary conditions at $z=h$ are

$$J_c(h) = R_{sc}I_c(h) \tag{46}$$

$$J_d(h) = R_{sd}I_d(h). \tag{47}$$

Substituting equations (5) and (6) in equations (44) and (46) and isolating

$$c_1 = \frac{(1-r_{c12})fI}{1-r_{c12}R_{sc}\mathrm{e}^{-2\zeta h}} \tag{48}$$

$$c_2 = \frac{(1-r_{c12})fIR_{sc}\mathrm{e}^{-2\zeta h}}{1-r_{c12}R_{sc}\mathrm{e}^{-2\zeta h}}. \tag{49}$$

Likewise, expressions for c_3 and c_4 are found substituting equations (7) and (8) in equations (45) and (47). After some lengthy but straight-forward algebra we find

$$c_3 = \sigma_1 fI + \sigma_2(1-f)I \tag{50}$$

$$c_4 = \sigma_3 fI + \sigma_4(1-f)I, \tag{51}$$

where

$$\begin{aligned}\sigma_1 = &\left\{\left[A[(C+BR_{sc}) - R_{sd}(B+CR_{sc})]\mathrm{e}^{-\zeta h}\right]\right.\\ &+\left[AR_{sd}\cosh(Ah) + (E-R_{sd}D)\sinh(Ah)\right]\\ &\left.\times\left[(C-r_{d21}B)R_{sc}\mathrm{e}^{-2\zeta h} + (B-r_{d21}C)\right]\right\}\\ &\times(1-r_{c12})\left[(1-r_{c12}R_{sc}\mathrm{e}^{-2\zeta h})(A^2-\zeta^2)DEN\right]^{-1}\end{aligned} \tag{52}$$

$$\sigma_2 = \frac{(r_{d12}-1)[AR_{sd}\cosh(Ah) + (E-R_{sd}D)\sinh(Ah)]}{DEN} \tag{53}$$

$$\begin{aligned}\sigma_3 = &\left\{\left[(D-r_{d21}E)\left[(C+BR_{sc}) - R_{sd}(B+CR_{sc})\right]\mathrm{e}^{-\zeta h}\right]\right.\\ &-\left[(E-R_{sd}D)\cosh(Ah) + AR_{sd}\sinh(Ah)\right]\\ &\left.\times\left[(C-r_{d21}B)R_{sc}\mathrm{e}^{-2\zeta h} + (B-r_{d21}C)\right]\right\}\\ &\times(1-r_{c12})\left[(1-r_{c12}R_{sc}\mathrm{e}^{-2\zeta h})(A^2-\zeta^2)DEN\right]^{-1}\end{aligned} \tag{54}$$

$$\sigma_4 = \frac{(1-r_{d12})[(E-R_{sd}D)\cosh(Ah) + AR_{sd}\sinh(Ah)]}{DEN}. \tag{55}$$

Reflectance, Transmittance, Absorptance

The total reflectance has an specular and a diffuse contribution. The specular contribution is the ratio of collimated reflected intensity to the total incident intensity

$$\mathcal{R}_c = \frac{r_{c12}fI + (1-r_{c12})J_c(0)}{I}. \tag{56}$$

Substituting equations (6) and (49) in equation (56), equation (17) is obtained. Analogously, the diffuse contribution

$$\mathcal{R}_d = \frac{r_{d12}(1-f)I + (1-r_{d21})J_d(0)}{I}. \tag{57}$$

Substituting equations (7), (38), (39), (48) and (50) in equation (57) and isolating the contribution from the collimated and diffuse incident light we obtain equations (18) and (19), where

$$C_0 = A[(C+BR_{sc}) - R_{sd}(B+CR_{sc})] \tag{58}$$

$$\begin{aligned}C_1 = &[A(BR_{sd}-C)\cosh(Ah)\\ &+[B(E-DR_{sd}) + C(ER_{sd}-D)]\sinh(Ah)]\end{aligned} \tag{59}$$

$$\begin{aligned}C_2 = &R_{sc}[A(CR_{sd}-B)\cosh(Ah)\\ &+[C(E-DR_{sd}) + B(ER_{sd}-D)]\sinh(Ah)]\end{aligned} \tag{60}$$

As well as the reflectance, the transmittance has also an specular and a diffuse contribution. In this case, the specular (diffuse) contribution is given by the sum of all the transmitted collimated (diffuse) rays originated due to multiple reflections within the substrate divided by the total incident intensity.

$$\mathcal{T}_c = T_{sc}\frac{I_c(h)}{I} = \left[\frac{(1-r_{c23})(1-r_{c34})\tau_c}{(1-r_{c23}r_{c34}\tau_c^2)}\right]\frac{I_c(h)}{I} \tag{61}$$

$$\mathcal{T}_d = T_{sd}\frac{I_d(h)}{I} = \left[\frac{(1-r_{d23})(1-r_{d34})}{1-r_{d32}r_{d34}\tau_d^2}\right]\frac{I_d(h)}{I}. \tag{62}$$

Substituting equation (5) in equation (61) and equation (8) in equation (62) and isolating the different contributions we get equations (20) to (22), where

$$D_1 = A\left[(r_{d21}C - B) + R_{sc}(r_{d21}B - C)\right] \tag{63}$$

$$D_2 = (E - r_{d21}D)(C + BR_{sc}) - (D - r_{d21}E)(B + CR_{sc}) \tag{64}$$

$$D_3 = A(B - r_{d21}C) \tag{65}$$

$$D_4 = AR_{sc}(C - r_{d21}B). \tag{66}$$

As stated in section 2, the total absorptance may be split up into two contributions, one arising from the absorption within the film and the other within the substrate. The absorption at the substrate, $\mathcal{A}_s$, can be evaluated from

$$\mathcal{A}_s = \frac{A_d I_d(h) + A_c I_c(h)}{I}, \tag{67}$$

where A_d and A_c are the diffuse and collimated light absorbed inside the substrate, given by

$$\begin{aligned}A_d &= 1 - R_{sd} - T_{sd}\\ &= \frac{(1-r_{d23})(1-\tau_d) + r_{d34}\tau_d(1-\tau_d-r_{d23}\tau_d)}{1-r_{d32}r_{d34}\tau_d^2}\end{aligned} \tag{68}$$

$$\begin{aligned}A_c &= 1 - R_{sc} - T_{sc}\\ &= \frac{(1-r_{c23})(1-\tau_c) + r_{c34}\tau_c(1-\tau_c-r_{c23}\tau_c)}{1-r_{c23}r_{c34}\tau_c^2}.\end{aligned} \tag{69}$$

Substituting equations (5), (8), (68) and (69) in equation (67), we obtain the expressions for $\mathcal{A}_s$ given in equations (27) to (29).

B. PARAMETERS OF THE FOUR-FLUX MODEL

The four-flux model requires many parameters whose values are not trivial. Thus in this appendix we review the physics behind each of them.

Average pathlength parameter

The average pathlength parameter ξ, also known as the average crossing parameter, provides the relative distance traveled by the diffuse light compared to collimated light. The value of ξ follows from its definition for two specific cases: under collimated radiation $\xi = 1$ and under perfectly diffuse incident radiation $\xi = 2$. However, ξ does not have to be constant. If the scattering is not isotropic, the assumption of a constant ξ constitutes a source of error within the model since the anisotropy between the angular distribution of the forward and backward diffuse radiation is not taken into account.

Mathematically, a light beam, whose direction forms an angle θ with the z-axis, travels a distance ΔL which is $1/\cos\theta$ larger than Δz, the distance traveled by a collimated beam. Averaging both sides over the intensity radiation field and integrating over the forward hemisphere the average pathlength can be evaluated with

$$\xi(z) = \frac{\int_0^1 I(z,\mu)\,\mathrm{d}\mu}{\int_0^1 \mu I(z,\mu)\,\mathrm{d}\mu}. \tag{70}$$

Due to the difficulty in evaluating equation (70) it has usually been considered constant [19] or as a fitting parameter. In certain cases there are explicit formulae for ξ, e.g., in the case of films containing spherical particles in a nonabsorbing matrix [33], in other cases its value has been studied with numerical methods [34]. We have set this parameter to $\xi = 2$ to avoid complications.

Scattering and absorption coefficients per unit length

The relative energy lost by a collimated beam flowing perpendicularly to an infinitesimal slab dz due to scattering (absorption) is related to the scattering (absorption) coefficient by $\alpha\,\mathrm{d}z$ ($\beta\,\mathrm{d}z$). In general, α and β depend on the properties of the material and are usually phenomenological parameters. In the case of a nonabsorbing medium with homogeneous spherical inclusions α and β can be evaluated from Mie-Lorenz theory

$$\alpha = \frac{\eta}{V} C_{\mathrm{sca}}\,, \tag{71}$$

$$\beta = \frac{\eta}{V} C_{\mathrm{abs}}\,, \tag{72}$$

where η is the filling fraction, V is the particle volume and, C_{sca} and C_{abs} are the scattering and absorption cross sections of the inclusions [23].

Forward scattering ratios

The forward scattering ratio is simply the relative amount of light scattered in the forward hemisphere within the media. This value is different for collimated (σ_c) and diffuse light (σ_d). In the case of collimated light, σ_c equals the amount of light scattered in the forward direction over the total scattered light, which can be evaluated using

$$\sigma_c = \frac{\int_0^1 p(\mu)\,\mathrm{d}\mu}{\int_{-1}^1 p(\mu)\,\mathrm{d}\mu}\,, \tag{73}$$

where $p(\mu)$ is the phase function. In the case of diffuse light the evaluation is more cumbersome since the forward hemisphere with respect to the beam direction does not coincide with the medium's forward hemisphere. σ_d is commonly evaluated numerically but there are analytical expressions for specific cases, e.g., a non-absorbing medium with absorbing-scattering particles [20].

The assumption that $\sigma_c = \sigma_d$ has been made [19]. This approximation does not hold except for limit cases such as isotropic scattering. We have assumed this configuration, hence the values $\sigma_c = \sigma_d = 0.5$ have been used in all computations.

Reflectances at the interfaces

Usually we have information relative to the refractive indices of the different media rather than the reflectances at each interface. However, these magnitudes are easily related by the Fresnel equation. The reflectance at the interface between medium i and medium j for a light beam with angle of incidence θ_i is

$$r_s(\theta_i) = \left| \frac{n_j \cos\theta_i - n_i \cos\theta_j}{n_j \cos\theta_i + n_i \cos\theta_j} \right|^2 \tag{74}$$

for parallel polarization and

$$r_p = \left| \frac{n_j \cos\theta_j - n_i \cos\theta_i}{n_j \cos\theta_j + n_i \cos\theta_i} \right|^2 \tag{75}$$

for perpendicular polarization, where n_i and n_j are the refractive indices of the media and θ_j is the angle of refraction which can be evaluated using the Snell law [35]. For unpolarized collimated light the reflectance at the interface is

$$r_{cij} = \frac{1}{2}\left(r_s + r_p\right) \tag{76}$$

with $\theta_i = \theta_p = 0$. In the case of diffuse light, multiple incident directions have to be taken into account. Therefore, we average the Fresnel factors over all possible angles of incidence [36]

$$r_{dij} = \frac{1}{2}\int_0^{\pi/2} \left[r_s(\alpha) + r_p(\alpha)\right] \sin(2\alpha)\,\mathrm{d}\alpha \tag{77}$$

Transmittances across the substrate

In addition to the absorption within the film, there can be absorption in the substrate. The substrate's absorption can be characterize by the transmittance τ across the substrate, i.e., the fraction of light that crosses the substrate without being absorbed. Since diffuse light covers more distance to travel the same distance than collimated light, $\tau_d \neq \tau_c$. The transmittance of a material is related to the attenuation coefficient, $\alpha(z)$, by the following expression

$$\tau = \exp\left(-\int_0^l \alpha(z)\,\mathrm{d}z\right), \tag{78}$$

where l is the material's length. Assuming constant attenuation over the whole substrate, i.e., a constant attenuation coefficient, the substrate's internal collimated and diffuse transmittances are related by

$$\tau_d = \tau_c^{\xi}\,. \tag{79}$$

We have applied this relationship throughout all the paper.

REFERENCES

1. A. Schuster, "Radiation through a foggy atmosphere," The Astrophys. J. **21**, 1–22 (1905).
2. Y. Zhang and J. C. Tan, "Radiation transfer of models of massive star formation. I. Dependence on basic core properties," The Astrophys. J. **733**, 55–75 (2011).
3. C. Emde, R. Buras-Schnell, A. Kylling, B. Mayer, J. Gasteiger, U. Hamann, J. Kylling, B. Richter, C. Pause, T. Dowling *et al.*, "The libRadtran software package for radiative transfer calculations (version 2.0. 1)," Geosci. Model. Dev. **9**, 1647–1672 (2016).
4. L. G. Sokoletsky, V. P. Budak, F. Shen, and A. A. Kokhanovsky, "Comparative analysis of radiative transfer approaches for calculation of plane transmittance and diffuse attenuation coefficient of plane-parallel light scattering layers," Appl. Opt. **53**, 459–468 (2014).
5. J. Hovenier and C. Van der Mee, "Fundamental relationships relevant to the transfer of polarized light in a scattering atmosphere," Astron. Astrophys. **128**, 1–16 (1983).
6. S. Platnick, "Vertical photon transport in cloud remote sensing problems," J. Geophys. Res. Atmospheres **105**, 22919–22935 (2000).
7. S. Y. Kotchenova, E. F. Vermote, R. Matarrese, and F. J. Klemm Jr, "Validation of a vector version of the 6S radiative transfer code for atmospheric correction of satellite data. Part I: Path radiance," Appl. Opt. **45**, 6762–6774 (2006).
8. S. Chandrasekhar, *Radiative transfer* (Courier Corporation, 2013).
9. P. Mudgett and L. Richards, "Multiple scattering calculations for technology," Appl. Opt. **10**, 1485–1502 (1971).
10. P. Kubelka and F. Munk, "An article on optics of paint layers," Z. Tech. Phys **12**, 593–601 (1931).

11. L. Fukshansky and N. Kazarinova, "Extension of the Kubelka–Munk theory of light propagation in intensely scattering materials to fluorescent media," J. Opt. Soc. Am. **70**, 1101–1111 (1980).
12. W. E. Vargas and G. A. Niklasson, "Applicability conditions of the Kubelka-Munk theory," Appl. Opt. **36**, 5580–5586 (1997).
13. L. Yang and S. J. Miklavcic, "Revised Kubelka-Munk theory. III. A general theory of light propagation in scattering and absorptive media," JOSA A **22**, 1866–1873 (2005).
14. R. Alcaraz de la Osa, A. G. Alonso, D. Ortiz, F. González, F. Moreno, and J. Saiz, "Extension of the Kubelka-Munk theory to an arbitrary substrate: a Monte Carlo approach," JOSA A **33**, 2053–2060 (2016).
15. V. D.-M. Ž. Barbarić-Mikočević and K. Itrić, "Kubelka-Munk theory in describing optical properties of paper (I)," Tech. Gazette **18**, 117–124 (2011).
16. H. R. Kang, "Applications of color mixing models to electronic printing," J. Electron. Imaging **3**, 276–288 (1994).
17. J. Beasley, J. Atkins, and F. Billmeyer Jr, "Scattering and absorption of light in turbid media," in "ICES Electromagnetic Scattering," , vol. 63 (1967), vol. 63, pp. 765–785.
18. A. Ishimaru, *Wave propagation and scattering in random media*, vol. 2 (Academic Press New York, 1978).
19. B. Maheu, J.-N. Letoulouzan, and G. Gouesbet, "Four-flux models to solve the scattering transfer equation in terms of Lorenz-Mie parameters," Appl. Opt. **23**, 3353–3362 (1984).
20. W. E. Vargas and G. A. Niklasson, "Forward-scattering ratios and average pathlength parameter in radiative transfer models," J. Physics: Condens. Matter **9**, 9083–9096 (1997).
21. W. E. Vargas, "Generalized four-flux radiative transfer model," Appl. Opt. **37**, 2615–2623 (1998).
22. C. A. Arancibia-Bulnes and J. C. Ruiz-Suárez, "Average path-length parameter of diffuse light in scattering media," Appl. Opt. **38**, 1877–1883 (1999).
23. W. E. Vargas and G. A. Niklasson, "Pigment mass density and refractive index determination from optical measurements," J. Physics: Condens. Matter **9**, 1661–1670 (1997).
24. F. El Haber, X. Rocquefelte, C. Andraud, B. Amrani, S. Jobic, O. Chauvet, and G. Froyer, "Prediction of the transparency in the visible range of x-ray absorbing nanocomposites built upon the assembly of LaF 3 or LaPO 4 nanoparticles with poly (methyl methacrylate)," JOSA B **29**, 305–311 (2012).
25. L. Wang, J. I. Eldridge, and S. Guo, "Comparison of different models for the determination of the absorption and scattering coefficients of thermal barrier coatings," Acta Materialia **64**, 402–410 (2014).
26. K. Laaksonen, S.-Y. Li, S. Puisto, N. Rostedt, T. Ala-Nissila, C.-G. Granqvist, R. Nieminen, and G. A. Niklasson, "Nanoparticles of TiO_2 and VO_2 in dielectric media: Conditions for low optical scattering, and comparison between effective medium and four-flux theories," Sol. Energy Mater. Sol. Cells **130**, 132–137 (2014).
27. C. Rozé, T. Girasole, and A.-G. Tafforin, "Multilayer four-flux model of scattering, emitting and absorbing media," Atmospheric environment **35**, 5125–5130 (2001).
28. B. Maheu, J. Briton, and G. Gouesbet, "Four-flux model and a Monte Carlo code: comparisons between two simple, complementary tools for multiple scattering calculations," Appl. Opt. **28**, 22–24 (1989).
29. L. Simonot, R. D. Hersch, M. Hébert, and S. Mazauric, "Multilayer four-flux matrix model accounting for directional-diffuse light transfers," Appl. Opt. **55**, 27–37 (2016).
30. M. I. Mishchenko, "Vector radiative transfer equation for arbitrarily shaped and arbitrarily oriented particles: a microphysical derivation from statistical electromagnetics," Appl. Opt. **41**, 7114–7134 (2002).
31. J. W. Tunnell, A. S. Haka, S. A. McGee, J. Mirkovic, and M. S. Feld, "Diagnostic tissue spectroscopy and its applications to gastrointestinal endoscopy," Tech. Gastrointest. Endosc. **5**, 65–73 (2003).
32. F. P. Bolin, L. E. Preuss, R. C. Taylor, and R. J. Ference, "Refractive index of some mammalian tissues using a fiber optic cladding method," Appl. Opt. **28**, 2297–2303 (1989).
33. W. E. Vargas and G. A. Niklasson, "Forward average path-length parameter in four-flux radiative transfer models," Appl. Opt. **36**, 3735–3738 (1997).
34. C. Rozé, T. Girasole, G. Gréhan, G. Gouesbet, and B. Maheu, "Average crossing parameter and forward scattering ratio values in four-flux model for multiple scattering media," Opt. communications **194**, 251–263 (2001).
35. E. Hecht, *Optics* (Pearson Education, 2017), 5th ed.
36. H. J. Mcnicholas, "Absolute methods in reflectometry," Bureau Standards J. Res. **1**, 29 (1928).